Rigaku

X-ray Diffraction & Elemental Analysis

THE BRIDGE

MATERIALS ANALYSIS eNEWSLETTER
NOVEMBER 2013, ISSUE 5

Welcome

As you might imagine, competitors read each other's newsletters. A recent article in such a newsletter caught our attention and prompted us to make our own measurements to validate the accuracy of our SmartLab diffractometer. We are pleased to report in the accompanying White Paper that the SmartLab performed quite well, thank you, and we use this issue to share our results.

Rarely a week goes by that Rigaku is not exhibiting at or attending a conference of some type, somewhere in the world. As this issue of The Bridge is being prepared, we are attending the 13th Chinese and International Biophysics Congress in Nanchang, China. The excitement and enthusiasm of the young students is contagious and it is almost overwhelming to try and understand the advances that are being made in understanding life at a molecular level. Our challenge as an instrument company is to keep up with the dreams and visions that our current and future customers hold. It is a strong challenge but one that keeps us motivated and moving forward with our technology.

Enjoy the newsletter.

A bridge is often used to symbolize a connection or link between two places, and thus we felt The Bridge would be the perfect name for our eNewsletter, as we hope that it will act as a vehicle for the transmission of ideas and information between Rigaku and interested readers around the world.

And a bridge is a two-way structure, a concept that we will keep in mind as we not only provide information about Rigaku, but also report on interesting research and the associated laboratories around the world, publish technical book reviews that might help our readers in their work, and highlight general news topics that are of interest to many people involved in materials analysis.

Photo by Paul Swepston

Featured Rigaku Journal Article

Powder diffraction optics for SmartLab X-ray diffractometer

Rigaku's Cross Beam Optics (CBO) pioneered the concept of easy switching functionality between Bragg-Brentano focusing beam and parallel beam configurations. This article discusses an extension of the CBO concept: a Johansson $K\alpha 1$ monochromator for high-resolution reflection mode or, combined with existing CBO and CBO-E optics, converting the focusing beam to parallel and convergent beam, respectively, for transmission mode diffraction experiments. The Johansson monochromator is mounted on a vertical θ-θ goniometer and the diffractometer can easily be switched to a non-Johansson configuration using the Guidance software, which guides the user to configure the proper setup and aligns the optics automatically.

Click here to see full article

Technical Discussion:

Ultra high-accuracy SmartLab goniometer

For thin film and powder diffraction measurements, the accuracy of the measurement is strongly influenced by the precision of the goniometer. The SmartLab's goniometer is a θ-θ vertical goniometer. The two θ axes are driven by AC servo motors and each goniometer angle is measured by a direct optical encoding system that is mounted directly on each goniometer gear. The result of this advanced mechanical design is that the SmartLab's goniometer achieves absolute angular accuracy of less than ±0.01° and minimum peak FWHM on NIST SRM 660b (LaB_6) below 0.025°.

The goniometer is designed to hold mechanical components weighing more than 30 kg so that it is able to be equipped with a heavy X-ray source, e.g. rotating anode generator, optics, e.g. Johansson $K\alpha_1$ optics, and detector, e.g. Pilatus 100K 2-D detector. Unlike some goniometers, it is not necessary to fix the θ axis even when it is configured in a high-resolution Johansson $K\alpha_1$ setup and it still can be operating in a θ-θ mode.

One of the parameters that indicate the goniometer precision is a minimum achievable peak FWHM (full width at half maximum) of a diffraction peak profile. In this article, peak profile measurements on a NIST SRM 660b (LaB_6) standard sample using the SmartLab X-ray diffractometer equipped with a 2 kW sealed X-ray tube and a 9 kW rotating anode generator will be discussed.

Figure 1 shows the SmartLab goniometer equipped with a 9 kW rotating anode generator, reflection sample stage and D/teX Ultra 250 1-D silicon strip detector. The primary optic configuration is Rigaku's CBO (Cross Beam Optics), which enables one to switch between Bragg-Brentano and parallel beam without optic alignment. In the experiments discussed here, the Bragg-Brentano configuration was used. The beam size and divergence is shaped by a motorized divergence slit, Soller slit and beam height limiting slit. The NIST SRM 660b sample was prepared on a reflection powder sample holder and mounted on the standard sample attachment. Diffracted X-rays were recorded utilizing a configuration of secondary optics including 2x motorized slits, anti-scattering slit and receiving slit, Soller slit and detector.

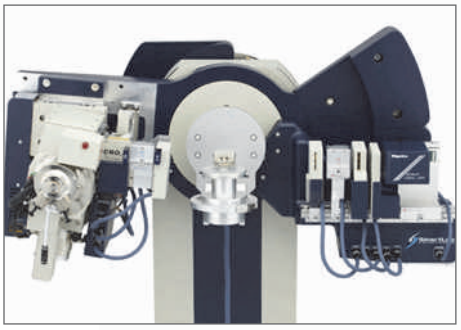

Figure 1. SmartLab X-ray diffractometer employed in the experiment. It is equipped with the new D/teX Ultra 250 1-D silicon strip detector. Note the instrument in the photograph is equipped with a 9kW rotating anode generator.

Figure 2 shows the 2θ-θ scan profile obtained for LaB_6 *100* diffraction peak. In this experiment, a copper sealed X-ray tube with 1.2 kW loading and a D/teX Ultra 250 1-D detector was used. Detailed scan conditions including optic configuration are summarized in Table 1.

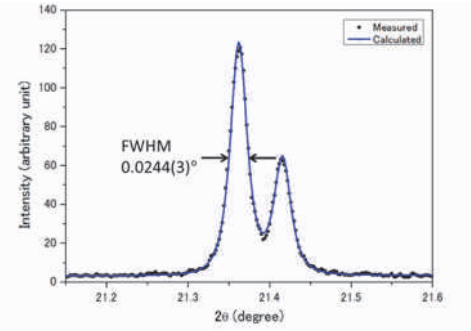

Figure 2. 2θ-θ scan result on NIST ASM660b (LaB_6) recorded by SmartLab X-ray diffractometer with Bragg-Brentano configuration with D/teX Ultra 250 1-D silicon strip detector.

The measured FWHM of the peak was 0.0244°. The FWHM was calculated by a profile-fitting algorithm using a split Pearson VII function implemented in Rigaku's PDXL software. To obtain such a very narrow peak, it is important to reduce the horizontal and axial divergence. For this reason, a relatively narrow divergence slit of 1/8° and a 0.5° Soller slit was used. Moreover, minimization of the defocussing effect is another important issue when a 1-D detector is used. The defocussing effect can be controlled by 2x slits on the secondary beam side, anti-scattering slit and the receiving slit. In this experiment, those slits were set to 3.0°.

Parameter	Value
X-ray source	1.2KW (Cu)
Divergence slit (°)	1/8
Primary soller slit (°)	0.5
Height limiting slit (mm)	2.0
Antiscattering slit (mm)	3.0
Receiving slit (mm)	3.0
Secondary soller slit (°)	0.5
Detector	D/teX Ultra 250
Step size (°)	0.0020
Scan speed (°/min.)	0.1/6

Table 1. Measurement conditions of the 2θ-θ scan shown in Figure 1.

Figure 3 shows the 2θ-θ scan profile of the LaB_6 *100* diffraction peak measured by a copper rotating anode X-ray generator running at 9.0 kW and utilizing a scintillation detector. Detailed scan conditions including the optic configuration are summarized in Table 2.

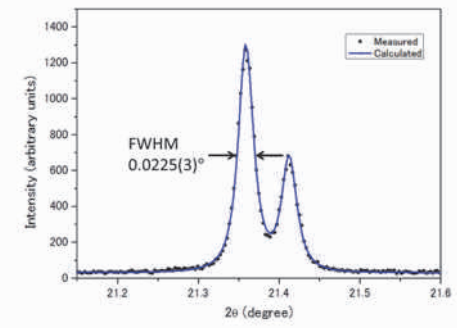

Figure 3. 2θ-θ scan result on NIST ASM660b (LaB_6) recorded by SmartLab X-ray diffractometer with Bragg-Brentano configuration with scintillation detector.

The FWHM of the measured peak was 0.0225°. As discussed earlier, control of both horizontal and axial divergence is important in obtaining such a narrow peak profile. For the secondary beam side, reducing the receiving slit is an important issue when the point detector (0-D detector) is used. In the experiment, a 0.05 mm receiving slit was used.

Parameter	Value
X-ray source	9.0KW (Cu)
Divergence slit (°)	1/6
Primary soller slit (°)	0.5
Height limiting slit (mm)	10.0
Antiscattering slit (°)	1/6
Receiving slit (mm)	0.05
Secondary soller slit (°)	0.5
Detector	Scintillation detector
Step size (°)	0.0028
Scan speed (°/min.)	0.007

Table 2. Measurement conditions of the 2θ-θ scan shown in Figure 2.

In conclusion, we have demonstrated that the SmartLab X-ray diffractometer has a goniometer with extraordinarily high accuracy. Minimum peak FWHM on NIST SRM 660b (LaB_6) was below 0.025° for both the 3 kW sealed X-ray tube system and the 9 kW rotating anode generator system. These results also indicate that the SmartLab goniometer is mechanically rigid enough to support a relatively heavy rotating anode generator. Moreover, obtained peak FWHM was almost the same when measured with a 1-D D/teX Ultra 250 detector as well as the 0-D scintillation detector. This demonstrates that the resolution of the D/teX Ultra 250 detector is quite high and equivalent to a point detector when operated with a narrow 0.05 mm receiving slit.

Click here for more information on the Rigaku SmartLab

Featured Application Note

WDXRF: Silicate Rock Analysis by the Low Dilution Fusion Method

The measurement of geochemical data from silicate rock is essential for modern petrology. WDXRF is a popular method for the determination of major elements, in silicate rock, using the fusion method for sample preparation. For measurement of the trace elements the pressed powder method is often used because dilution by flux significantly reduces sensitivities. This application note describes a low dilution fusion method that allows both major elements and trace elements to be measured accurately from one sample.

Click here to see full application note

To learn more about the Rigaku MiniFlex benchtop X-ray diffractometer, watch the product overview video above.

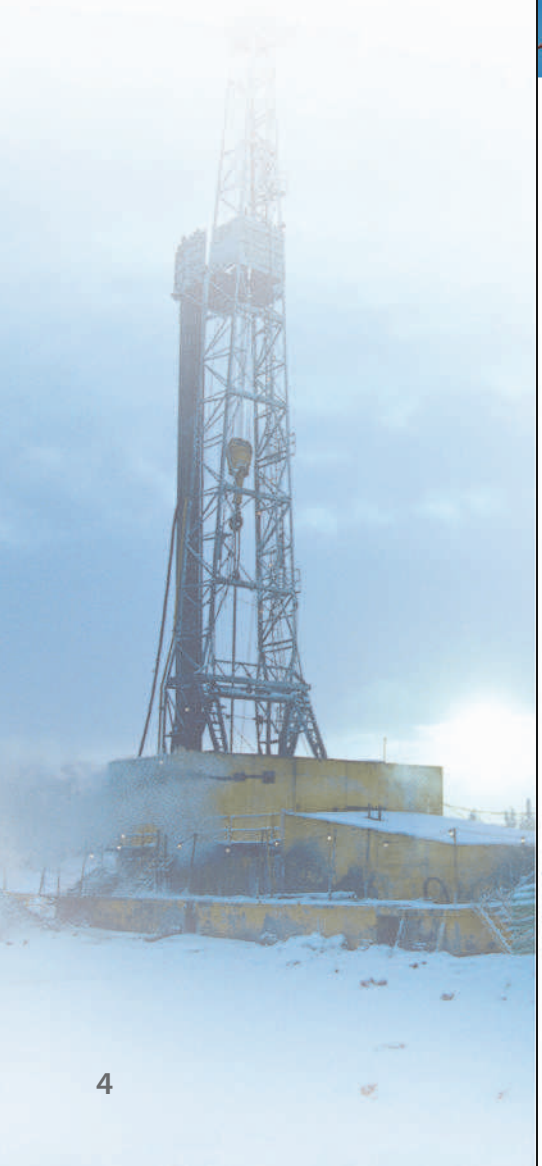

Cluster Analysis – A High-Throughput X-ray Diffraction Method for Mineral Identification and Quantification

by Lori Hatherley, Rigaku Americas Corporation

Abstract

Due to increased activity from oil and gas drilling sites, many mineral laboratories are facing a significant increase in the number of core, scale and corrosion samples, along with a corresponding demand for faster turn-around time. New methodologies to increase efficiency and provide faster results are necessary to meet client expectations. Cluster analysis can be utilized as a high-throughput method with a shorter analysis time than current X-ray diffraction testing procedures to confirm the mineralogy of each stratum in the drilling process. Cluster analysis results are compared to traditional methods from existing core labs in two cases studies of varying oil field shale and scale samples. **One study consists of 21 bulk mineral core samples** (FTS International Corporation). Core samples from neighboring wells are sampled at varying depths.

The second case study consists of 33 scale and corrosion samples (Baker Hughes Upstream Chemical Analytical Laboratories). Although many samples in this study are unusual, similarities and efficacies are discovered. In both cases, analysis time can be significantly decreased.

Cluster analysis with Rigaku's PDXL program allows users to pre-sort large sets of X-ray diffraction data into clusters of similarity based on Principal Component Analysis (PCA). Cluster results are displayed visually in dendrograms separated by Eigenvalues of similarity. Picking the most similar patterns allows pre-separation of data to increase efficiency in analysis.

Case Study of Well Samples - 21

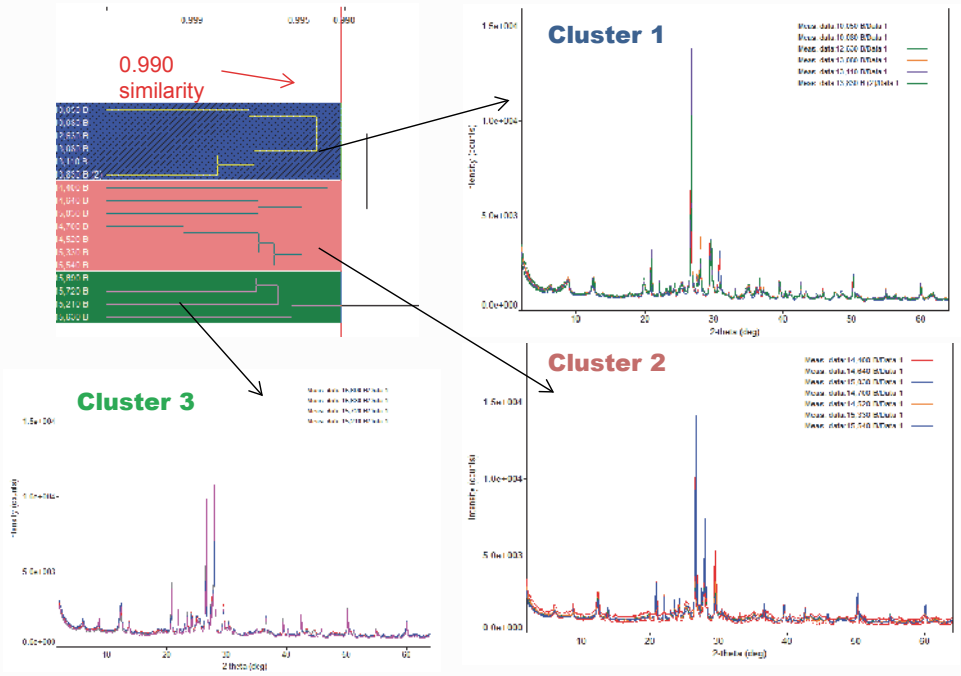

Figure 1. By choosing an Eigenvalue of 0.990 similarity criteria, three groups appeared in the dendrogram.

	10.050 B
Method	WPPF
Quartz(%)	20.5(4)
Calcite, magnesium, syn(%)	12.1(5)
Muscovite 2M1(%)	25.1(19)
dolomite(%)	7.3(6)
Clinochlore-1MIIb, ferroan(%)	12.7(9)
Albite, calcian(%)	13.3(10)
Labradorite(%)	1.4(10)
Aragonite(%)	4(2)
Cristobalite(%)	2.3(2)

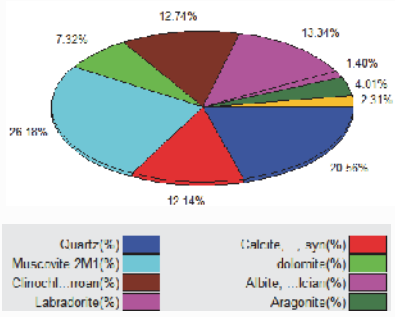

Figure 2. In Cluster 1, sample 10050 is used to create a template for phase identification and quantification. Results are displayed above.

	10,080 B	12.630 B	13,080 B	13,110 B	13,830 B (2)
Method	WPPF	WPPF	WPPF	WPPF	WPPF
Quartz(%)	19.2(4)	20.1(3)	20.2(3)	17.5(3)	18.8(4)
Calcite, magnesium	15.0(6)	7.1(7)	6.6(8)	8.0(6)	12.8(6)
Muscovite 2M1(%)	20(3)	35.9(11)	37.0(14)	27.5(14)	36(3)
Clinochlore-1MIIb, fe	6.1(12)	8(4)	4.0(8)	9.9(12)	13.1(19)
Illite-1M (NR)(%)	11.7(16)	17(3)	2(3)	11(8)	5(5)
dolomite(%)	13.0(8)	0.7(15)	4.3(17)	2.9(5)	0(2)
Albite, calcian(%)	11.6(13)	5.7(10)	20.1(7)	8.2(5)	14.3(11)
Labradorite(%)	0(5)	3.6(11)	3.4(8)	1.9(4)	0(5)
Cristobalite(%)	0.3(12)	1.1(3)	0.0(10)	5.1(9)	0.0(9)
pyrite, syn(%)	1.7(2)	1.44(11)	2.2(3)	7.7(9)	0(5)

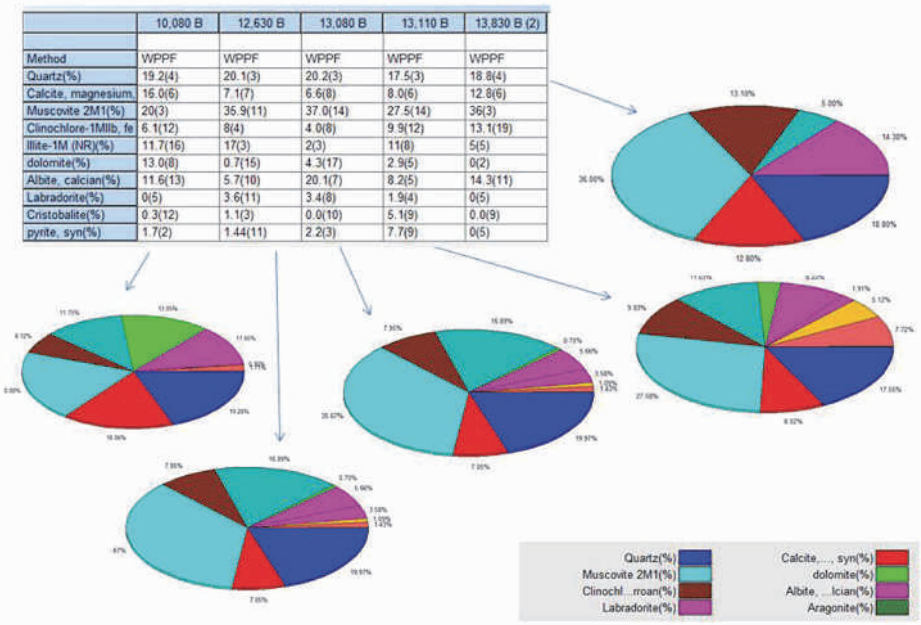

Figure 3. Once a template is established, open remaining cluster data and process for phase identification and quantification by the Rietveld method. Results are displayed above.

XRD for Everyone

Benchtop qualitative and quantitative powder diffraction

The 5th generation MiniFlex is a general purpose X-ray diffractometer that can perform qualitative and quantitative analysis of polycrystalline materials. The MiniFlex is available in two variations. Operating at 600 watts (X-ray tube), the MiniFlex 600 is twice as powerful as other benchtop models, enabling faster analysis and improved overall throughput. Running at 300 watts (X-ray tube), the new MiniFlex 300 does not require an external heat exchanger. Each model is engineered to maximize flexibility in a benchtop package.

Click here for more information on the Rigaku MiniFlex

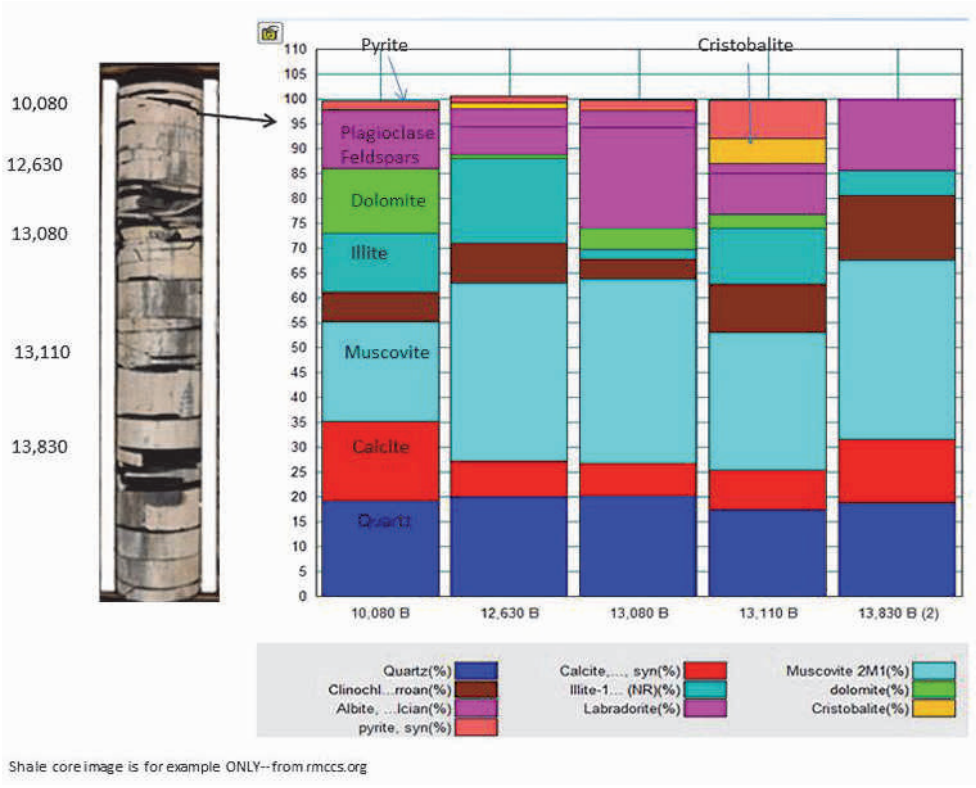

Figure 4. Alternative view for Rietveld quantitative analysis. This format can be used to monitor the trends in phase changes by depth.

Summary:

Case Study 1:
Original time for analyzing the data was 3.5 hours per sample. Using Rigaku's Cluster Analysis Software, analysis time per sample can be decreased to 13 minutes. For brevity, 17 of the 21 sample results are displayed above.

As well as saving vast amounts of time, results from Rigaku's Cluster Analysis software correlate well to the original analysis report. Cluster results are within 8 wt. percent for 48% of the samples, 12 wt. percent for 43% of the samples and within 20 wt. percent for the remaining 9% of the original data sets.

Case Study of Scale And Corrosion Samples - 33

For example, below is a set of 14 scale and corrosion samples. Geological raw XRD patterns were analyzed using Cluster Analysis method by peak list (from template).

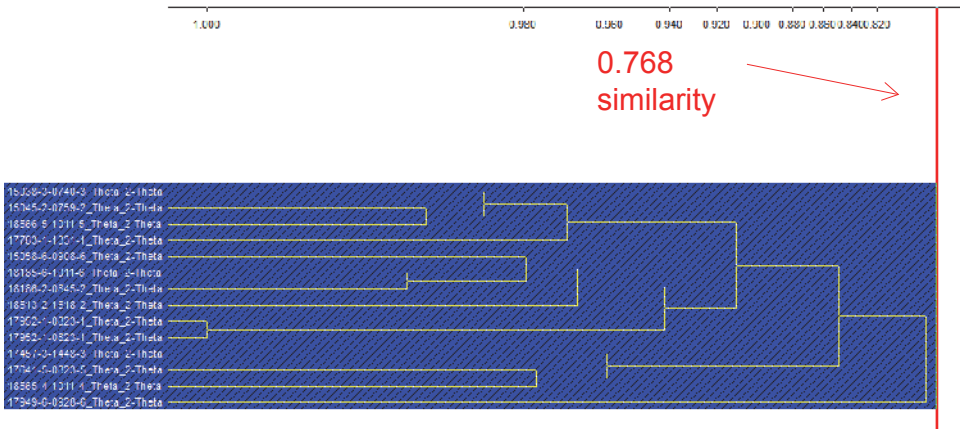

Figure 5. All samples had an Eigenvalue of 0.768 similarity. This indicates a significant amount of diversity or little similarity.

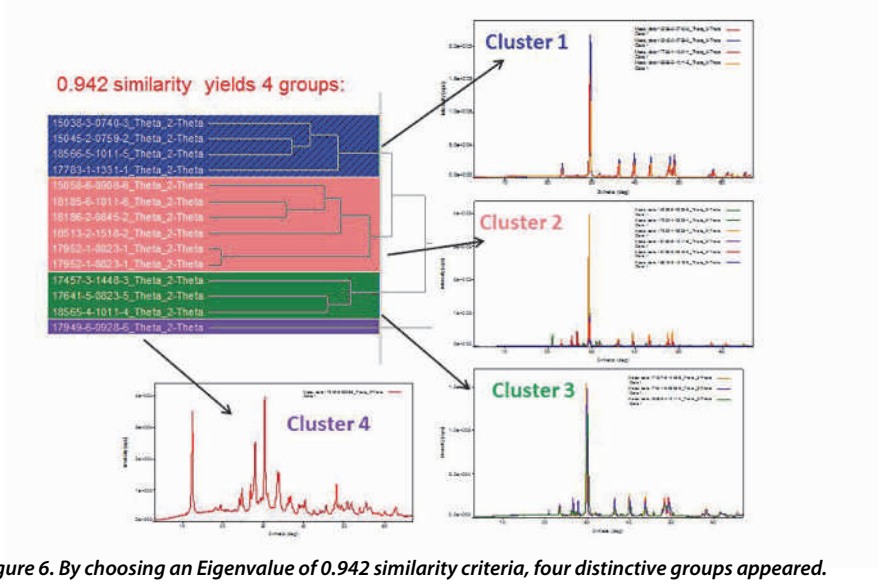

Figure 6. By choosing an Eigenvalue of 0.942 similarity criteria, four distinctive groups appeared.

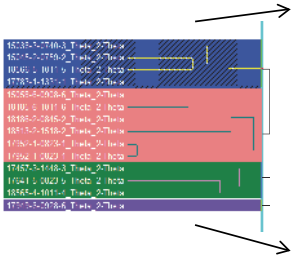

Wt%	calcite	quartz	dolomite	barite	others
15038	**100**				
15045	**98.43**	1.26			KCl 0.21
18566	**93.3**				
17783	**99.81**				Celsian (BaALSiO2-
15058	**69**	**21**	11		halite- 5.0, siderite-6.0; rudashevskyite-0.7
18185	**82**	**7**		5.4	halite-1.9, kaotite-4.0; fersilicite -0.22
18186	**71**	**21**		3	halite-4.2, kaotite-01; fersilicite -0.24
18513	**76.92**	**7.16**			halite- 1.07, goethite-8, .68, gypsum-6.17
17952	**98**	**0.94**		0.26	halite-0.3, kaotite-0.47; fersilicite -0.11
17457	98.25				**halite-0.95, iron- 0.8**
17641	86.91	7.8			**kspar-2.70; plagioclases-3.70**
18565	75 ($CaMnCO_3$);				**aragonite- 11.4; sylivine(KCl)-1.7; Sanidine 11.7**
17949	Calcite- 86 monoclinic 1.5 GPa	4			phillipsite-5 (Ba-feldspar); hematite-1,

Figure 7. Each group was selected and analyzed for phase identification and quantitative analysis (using Rietveld or RIR where crystal structures were unavailable).

Discussions:

Results have been entered into a spreadsheet with coordinating colors to show the reasons for grouping. All groups contained at least calcite, but group 1 contained all pure calcite phases (100 to 98%) with very little other trace phases. Group 2 contained calcite (98 to 69%) with minor phases of quartz and halite trace phases. Group 3 contained predominately calcite (substituted with some Mg) and with different trace phases. Group 4 was a pressure altered calcite with varying trace phases.

Next **set of 19 scale** and corrosion samples. Geological raw XRD patterns were analyzed using Cluster Analysis method by peak list (from template).

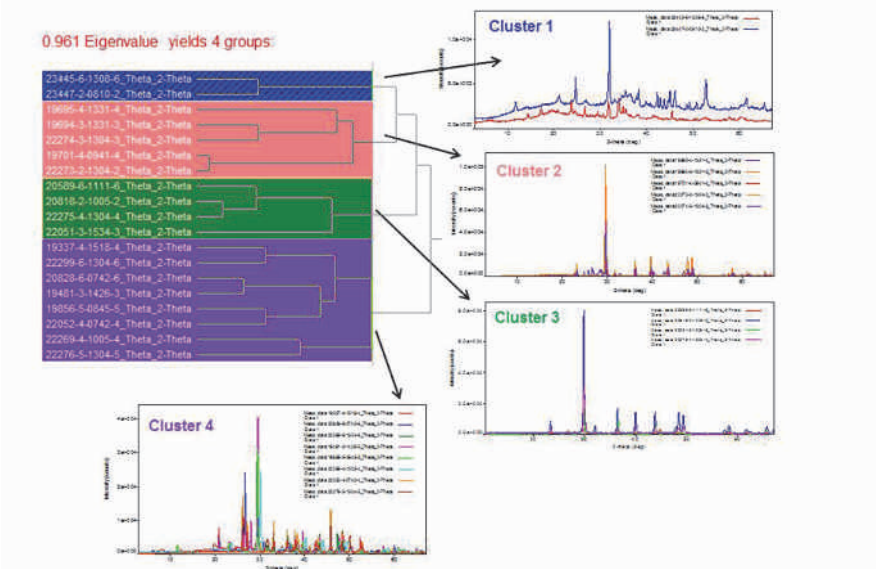

Figure 8. By choosing an Eigenvalue of 0.961 similarity criteria, four distinctive groups appeared.

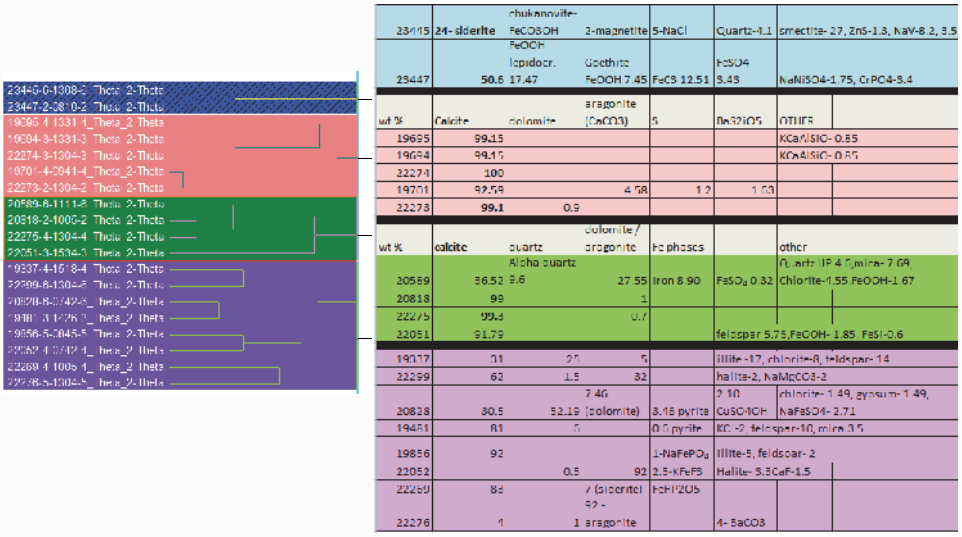

23415	24- siderite	chukanovite-FeCO3OH	2-magnetite	5-NaCl	Quartz-4.1	smectite- 27, ZnS-1.3, NaV-8.2, 3.5
23447	50.6	FeOOH lepidocr. 17.47	Goethite FeOOH 7.45	FeCS 12.51	FeSO4 3.45	NaNiSO4-1.75, CrPO4-3.4
wt %	Calcite	dolomite	aragonite (CaCO3)	S	Na2UO5	OTHER
19695	99.15					KCaAlSiO- 0.85
19684	99.15					KCaAlSiO- 0.85
22274	100					
19701	92.59		4.58	1.2	1.63	
22273	99.1	0.9				
wt %	calcite	quartz	dolomite / aragonite	Fe phases		other
		Alpha quartz				Quartz-LP 4.5,mica- 7.69,
20589	36.53	9.6	27.55	Iron 8.90	$FeSO_4$ 0.32	Chlorite-1.55 FeOOH-1.67
20818	99		1			
22275	99.4		0.7			
22051	91.79					feldspar 5.75,FeOOH- 1.85, FeSi-0.6
19917	91	2?	7		illite -17, chlorite-8, feldspar- 14	
22299	62	1.5	32		halite-2, NaMgCO3-2	
20828	80.5	7.46 52.19 (dolomite)		3.15 pyrite	? 10 CuSO4OH	chlorite- 1.49, gypsum- 1.49, NaFeSO4- 2.71
19451	81	0		0.5 pyrite	KC- ?, feldspar-10, mica 2.5	
19856	92			1-$NaFePO_4$	illite-5, feldspar- 2	
22052		0.5	92	2.5-KFeFS	Halite- 3.3CaF-1.5	
22269	88		? (siderite) 92 -	FeHPO5		
22276	1		1 aragonite		4- BaCO3	

Figure 9. Each group was selected and processed. Significant similarities reduced the time for phase identification and quantitative analysis (using Rietveld or RIR where crystal structures were unavailable). Results have been entered into a spreadsheet with coordinating colors to show the reasons for grouping.

Summary:

Case Study 2:
Analysis time was 30 minutes for each sample using the original method of analysis. Analysis time decreased to 10 minutes with Rigaku's Cluster Analysis software but now includes quantitation (which was not performed in the original analysis).

Special thanks go to Researchers at ***FTS International, Houston, TX*** *and* ***Baker Hughes Upstream Chemical Analytical Laboratories, Bakersfield, CA*** *for providing the raw data patterns and support. All data patterns were collected with the* ***Rigaku MiniFlex 600 and D/teX Ultra high speed detector****.*

Join Rigaku at Future Meetings

Rigaku will be sponsoring, attending or exhibiting at the following conferences and trade shows:

Materials Research Society (MRS)
Boston, MA, USA, *December 1 – 6*

CPhI India
Mumbai, India, *December 3 – 5*

SEMICON Japan 2013
Chiba, Japan, *December 4 – 6*

Asian Crystallographic Association (AsCA)
Hong Kong, China, *December 7 – 10*

American Geophysical Union (AGU)
San Francisco, CA, USA, *December 9 – 13*

Rigaku exhibited (photo above) at the 13th Chinese and International Biophysics Congress October 28 – November 1 in Nanchang, China. Over 1000 attendees demonstrated the growing importance of biophysics in China.

Click here to see the complete list

The Adventures of Captain Nano

Battling the N.I.B.s — Transfered to another lab by way of mop bucket, the Captain finds himself face to face with Nano Inorganic Bots intent on erasing his mind.

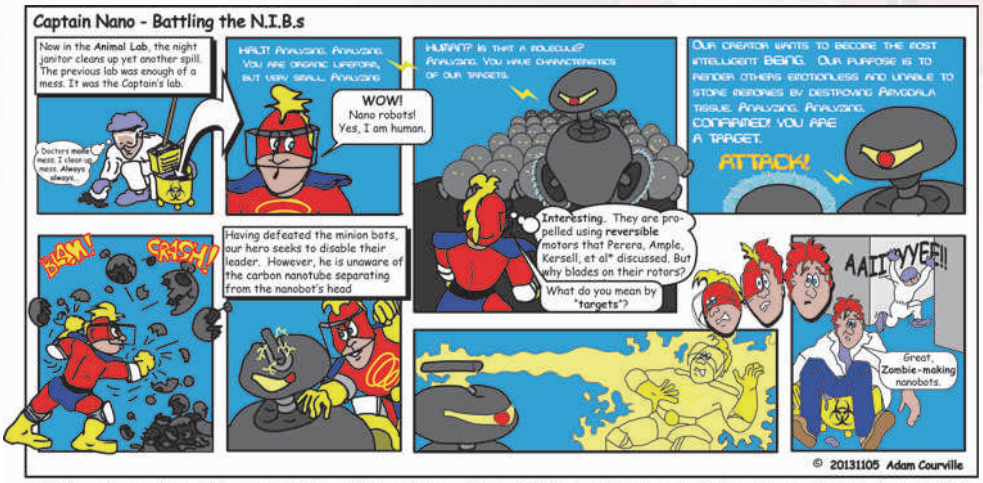

*U. G. E. Perera, F. Ample, H. Kersell, Y. Zhang, G. Vives, J. Echeverria, M. Grisolia, G. Rapenne, C. Joachim & S-W. Hla. Controlled clockwise and anticlockwise rotational switching of a molecular motor (2013) *Nature Nanotechnology* 8, 46–51

Material Analysis in the News

News for November 2013

November 6, 2013. Using the world's most brilliant X-ray source, scientists have for the first time peered into molten magma at conditions of the deep Earth mantle. The analysis at DESY's light source PETRA III revealed that molten basalt changes its structure when exposed to pressure of up to 60 gigapascals (GPa), corresponding to a depth of about 1400 kilometres below the surface.

November 12, 2013. *X-ray fluorescence spectrometry and related techniques: an introduction.* This book is a tutorial providing an up-to-date description of the fundamentals of X-ray fluorescence (XRF) techniques including an overview of instrumentation, sample preparation procedures and applications. Readers new to XRF analysis will benefit from the straightforward writing style, and more established X-ray analysts will gain from the description of related techniques.

November 12, 2013. Stephen "Steve" Wilkins was a distinguished physicist with CSIRO and adjunct professor at Monash University. He passed away suddenly, as he was about to deliver the first in a series of lectures on X-ray science to physics honours students at Monash.

November 13, 2013. Using the X-ray beams of The European Synchrotron (ESRF) a team of international scientists showed that the electrons absorbed and released by cerium dioxide nanoparticles during chemical reactions behave in a completely different way than previously thought: the electrons are not bound to individual atoms but, like a cloud, distribute themselves over the whole nanoparticle.

November 15, 2013. For many centuries mercury sulfide was the painter's finest red pigment, but in some old paintings it has now darkened to a blackish color. The explanation has been controversial, but a research team using a combination of x-ray spectroscopy and first-principles calculations now claims to have discovered the photochemical processes responsible.

November 15, 2013. Hydrogenation of an aluminium alloy to create a novel material for hydrogen gas storage has been investigated using in situ synchrotron radiation X-ray diffraction measurements and other techniques pointing to a bright future for a once-luxury metal.

November 18, 2013. The first X-ray diffraction image of Martian soil was taken from the Gale crater. The soil revealed traces of feldspar, olivine and pyroxenes. James Wray, Assistant Professor in the School of Earth and Atmospheric Sciences at the Georgia Institute of Technology, and lead author of the new study, claims that his research team has yielded the "most compelling" evidence yet that Mars boasts granitic rocks.

November 20, 2013. Researchers from University College London (UCL) in the UK and INFN in Italy have developed a new gold nanoparticle (GNP) imaging method for tumors that works by detecting the L-edge X-ray fluorescence (L-XRF) emitted when gold is irradiated with 15 keV X-rays. The technique can achieve increased detection sensitivity at greater depths than current optical modalities. The INFN group designed two L-XRF imaging systems; a step-and-scan spectroscopic module and an energy-resolving pixellated detector.

November 20, 2013. Martin de Jonge from The Australian Synchrotron in Clayton Victoria has entered The Australian Innovation Challenge with a project probing the distribution of nutrients in food and the environment using an X-ray fluorescence microprobe at the Australian Synchrotron.

Scientific Book Review

***The Spark of Life* By Frances Ashcroft**

In her newest book, *The Spark of Life*, Oxford professor Frances Ashcroft looks at the role of electricity in the human body. Ashcroft begins by looking at perceptions of electricity's role in the human body in popular culture, and inevitably touches upon the resurrection of Victor Frankenstein's monster in Mary Shelley's eponymous novel. Ashcroft points out that, though Shelley's story is obviously one of fiction, Shelley based her idea for the creation of life on research being conducted by her contemporaries. Scientists now know that electrical transmissions in the human body are facilitated by proteins in cell membranes known as ion channels. A number of neurological disorders stem from genetic mutations that lead to alterations in the structures of these membrane proteins, which in turn leads to inhibition or altercation in transmission. Ashcroft's research specialty is a particular ion channel, the KATP channel, which plays important roles not only in insulin secretion but brain function. Throughout her book, Ashcroft returns to her discussion of the KATP channel and its roles in the body.

Ashcroft's discussion of the role of electricity in the human body is balanced between explanations of everyday occurrences, such as why one receives a shock after shuffling across a carpeted floor on a dry, cold day, and more technical explanations of neurological phenomena. Perhaps my favorite discussion was that of neurotoxins found throughout the animal kingdom. The pufferfish is considered a delicacy in Japan, where it is known as fugu. However, if not cooked correctly it can prove fatal to the consumer, as the tetrodotoxin contained in most of the fish's tissues and organs is quite poisonous. A number of animals contain tetrodotoxin, including crabs, starfish, octopi, salamanders, frogs and toads; however, these animals do not actually produce the toxin. A bacterium, *Psuedoalteromonas tetraodonia*, harbors within the intestines of these animals and produces the toxin. What makes tetrodotoxin so dangerous is that it blocks the sodium channels in nerves and skeletal muscles, leading to paralysis—eventually paralysis of the respiratory muscles usually leads to death. Interestingly enough, the heart is not affected by tetrodotoxin—it has a different kind of sodium channel that the toxin does not target. Unfortunately, there is no antidote to the poison and death occurs in less than twenty-four hours, depending on the potency of the dose. The only way to survive is if artificial respiratory support is provided until the body cleanses itself of the toxin, which takes several days.

Ashcroft also discusses the role of electricity in human perception—the nervous system is inherently and intricately related with the "five senses"—taste, touch, sight, smell, and hearing. Negatively impacting the transmission of electrical impulses across cell membranes has a negative impact on the ability of human beings to perceive their surroundings. Ashcroft rounds out her discussion with a look to the future as far as electrical devices are concerned and their interactions with human bodies—some can be used to kill, but other, such as hearing aids, can be used to help counteract the physical effects of damaged sensory input/output systems.

At times Ashcroft could be a bit technical, but overall a good read; definitely enlightening and highly recommended.

Jeanette S. Ferrara
Princeton, Class of 2015.

Training Classes

Rigaku Americas Corp held concurrent training classes for XRD and XRF October 22 – 24 at its application facility in The Woodlands, Texas.

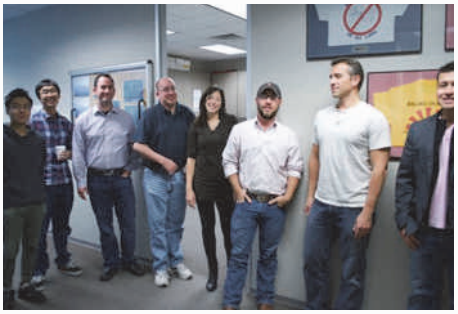

The XRF training session covered XRF theory and applications support and had 17 participants. The main instructor was Jeff Borgeson, who was supported by guest instructor, Lee Ann Moye. Additional Rigaku personnel in attendance were Glenn Williams and Ryan Nelson.

The XRD training session covered the MiniFlex 600 and PDXL software. There were 13 participants for the training classes and they were given hands on training on Rigaku's popular MiniFlex powder diffractometer. Lori Hatherly provided lively instruction as always.

The participants were treated to an al fresco Italian lunch feast on the second day in order to enjoy Houston's beautiful fall weather.

For more information about upcoming Rigaku training classes around the world, click here

Recent Scientific Papers of Interest

Feasibility study on the use of cellular concrete as alternative raw material for Portland clinker production. Schoon, Joris; De Buysser, Klaartje; Van Driessche, Isabel; De Belie, Nele. Construction & Building Materials. Nov2013, Vol. 48, p725-733. 9p. DOI: 10.1016/j.conbuildmat.2013.07.083.

Optical and Structural Properties of MEH-PPV: C60-Based Structures. Dhibi, Olfa; Ltaief, Adnen; Bouazizi, Abdelaziz. Fullerenes, Nanotubes & Carbon Nanostructures. 2013, Vol. 21 Issue 10, p894-900. 7p. DOI: 10.1080/1536383X.2013.826195.

Quantifying Three-Dimensional Residual Stress Distributions Using Spatially-Resolved Diffraction Measurements and Finite Element Based Data Reduction. Park, J.-S.; Lienert, U.; Dawson, P.; Miller, M. Experimental Mechanics. Nov2013, Vol. 53 Issue 9, p1491-1507. 17p. DOI: 10.1007/s11340-013-9771-0.

Nanoscale surface characterization of aqueous copper corrosion: Effects of immersion interval and orthophosphate concentration. Daniels, Stephanie L.; Sprunger, Phillip T.; Kizilkaya, Orhan; Lytle, Darren A.; Garno, Jayne C. Applied Surface Science. Nov2013, Vol. 285, p823-831. 9p. DOI: 10.1016/j.apsusc.2013.08.136.

Characterization of carbon nanotube webs and yarns with small angle X-ray scattering: Revealing the yarn twist and inter-nanotube interactions and alignment. Dumée, Ludovic; Sears, Kallista; Mudie, Stephen; Kirby, Nigel; Skourtis, Chris; Mcdonnell, Jill; Lucas, Stuart; Schütz, Jürg; Finn, Niall; Huynh, Chi; Hawkins, Stephen; Kong, Lingxue; Hodgson, Peter; Duke, Mikel; Gray, Stephen. Carbon. Nov2013, Vol. 63, p562-566. 5p. DOI: 10.1016/j.carbon.2013.06.065.

Chemical, mineralogical and morphological changes in weathered coal fly ash: A case study of a brine impacted wet ash dump. Eze, Chuks P.; Nyale, Sammy M.; Akinyeye, Richard O.; Gitari, Wilson M.; Akinyemi, Segun A.; Fatoba, Olanrewaju O.; Petrik, Leslie F. Journal of Environmental Management. Nov2013, Vol. 129, p479-492. 14p. DOI: 10.1016/j.jenvman.2013.07.024.

Improvement of the Contour Method for Measurement of Near-Surface Residual Stresses from Laser Peening. Toparli, M.; Fitzpatrick, M.; Gungor, S. Experimental Mechanics. Nov2013, Vol. 53 Issue 9, p1705-1718. 14p. DOI: 10.1007/s11340-013-9766-x.

Mechano optical behavior of polyethylene terephthalate films during simultaneous biaxial stretching: Real time measurements with an instrumented system. Hassan, M.; Cakmak, M. Polymer. Nov2013, Vol. 54 Issue 23, p6463-6470. 8p. DOI: 10.1016/j.polymer.2013.09.045.

Sodium dodecyl sulfate (SDS) effect on the thermal stability of oxy-HbGp: Dynamic light scattering (DLS) and small angle X-ray scattering (SAXS) studies. Carvalho, José Wilson P.; Alves, Fernanda Rosa; Batista, Tatiana; Carvalho, Francisco Adriano O.; Santiago, Patrícia S.; Tabak, Marcel. Colloids & Surfaces B: Biointerfaces. Nov2013, Vol. 111, p561-570. 10p. DOI: 10.1016/j.colsurfb.2013.06.050.

Residual stress relaxation and low- and high-cycle fatigue behavior of shot-peened medium-carbon steel. Kim, Jong-Cheon; Cheong, Seong-Kyun; Noguchi, Hiroshi. International Journal of Fatigue. Nov2013, Vol. 56, p114-122. 9p. DOI: 10.1016/j.ijfatigue.2013.07.001.

Characterisation of fractionated skim milk with small-angle X-ray scattering. Sørensen, Hanne; Pedersen, Jan Skov; Mortensen, Kell; Ipsen, Richard. International Dairy Journal. Nov2013, Vol. 33 Issue 1, p1-9. 9p. DOI: 10.1016/j.idairyj.2013.05.006.

Surface morphology of homoepitaxial *c*-plane GaN: Hillocks and ridges. Oehler, F.; Zhu, T.; Rhode, S.; Kappers, M.J.; Humphreys, C.J.; Oliver, R.A. Journal of Crystal Growth. Nov2013, Vol. 383, p12-18. 7p. DOI: 10.1016/j.jcrysgro.2013.07.035.

Improving gas hydrate saturation estimates using P-wave velocity log data by incorporating XRD-data for detailed matrix-mineralogy definition. Kim, H.-S.; Riedel, M.; Ryu, B.-J.; Kim, G.-Y.; Bahk, J.-J. Marine & Petroleum Geology. Nov2013, Vol. 47, p155-167. 13p. DOI: 10.1016/j.marpetgeo.2013.05.020.

Mineralogical Composition of Clinker as an Indicator of Sulfate Resistance: A Rietveld XRD/Takashima Approach. Robledo-Gutiérrez, Miriam; Blanco-Varela, María Teresa; Carmona-Quiroga, Paula María. Journal of the American Ceramic Society. Nov2013, Vol. 96 Issue 11, p3637-3642. 6p. 1 Color Photograph, 1 Black and White Photograph, 4 Charts, 6 Graphs. DOI: 10.1111/jace.12575.

Non-isothermal kinetics and *in situ* SR XRD studies of hydrogen desorption from dihydrides of binary Ti–V alloys. Suwarno, S.; Solberg, J.K.; Mæhlen, J.P.; Denys, R.V.; Krogh, B.; Ochoa-Fernández, E.; Børresen, B.T.; Rytter, E.; Gabis, I.E.; Yartys, V.A. International Journal of Hydrogen Energy. Nov2013, Vol. 38 Issue 34, p14704-14714. 11p. DOI: 10.1016/j.ijhydene.2013.08.103.

The double molybdate $Na_9Sc(MoO_4)_6$ refined from powder XRD data. Savina, Aleksandra A.; Morozov, Vladimir A.; Basovich, Olga M.; Khaikina, Elena G.; Lazoryak, Bogdan I. Acta Crystallographica: Section C (International Union of Crystallography - IUCr). Nov2013, Vol. 69 Issue 11, p1301-1303. 3p. DOI: 10.1107/S0108270113028862X.

Surface integrity after pickling and anodization of Ti–6Al–4V titanium alloy. Vermesse, Eric; Mabru, Catherine; Arurault, Laurent. Applied Surface Science. Nov2013, Vol. 285, p629-637. 9p. DOI: 10.1016/j.apsusc.2013.08.103.

Large thickness-dependent improvement of crystallographic texture of CVD silicon films on R-sapphire. Moyzykh, M.; Samoilenkov, S.; Amelichev, V.; Vasiliev, A.; Kaul, A. Journal of Crystal Growth. Nov2013, Vol. 383, p145-150. 6p. DOI: 10.1016/j.jcrysgro.2013.08.038.

Hierarchical modelling of elastic behaviour of human enamel based on synchrotron diffraction characterisation. Sui, Tan; Sandholzer, Michael A.; Baimpas, Nikolaos; Dolbnya, Igor P.; Landini, Gabriel; Korsunsky, Alexander M. Journal of Structural Biology. Nov2013, Vol. 184 Issue 2, p136-146. 11p. DOI: 10.1016/j.jsb.2013.09.023.

SEM, AFM, EDX and XRD analysis of laser ablated Ti in nonreactive and reactive ambient environments. Kalsoom, Umm-i; Bashir, Shazia; Ali, Nisar. Surface & Coatings Technology. Nov2013, Vol. 235, p297-302. 6p. DOI: 10.1016/j.surfcoat.2013.07.056.

Effects of carbon nanotubes addition on the composition and mechanical properties of $AlMgB_{14}$ ceramics. Liu, W; Miao, Y; Pan, RL; Zhang, J; Zhang, TM; Mao, SH. Journal of Composite Materials. Nov2013, Vol. 47 Issue 25, p3187-3193. 7p. DOI: 10.1177/0021998312463108.

Probing the Local Structure and Phase Transitions of $Bi_4V_2O_{11}$-Based Fast Ionic Conductors by Combined Raman and XRD Studies. Patwe, Sadequa J.; Patra, Atanu; Dey, Rita; Roy, Anushree; Kadam, Ramakant M.; Achary, Srungarpu N.; Tyagi, Avesh K. Journal of the American Ceramic Society. Nov2013, Vol. 96 Issue 11, p3448-3456. 9p. 4 Diagrams, 6 Charts, 9 Graphs. DOI: 10.1111/jace.12490.

X-ray diffraction without sample preparation: Proof-of-principle experiments. Hansford, Graeme M. Nuclear Instruments & Methods in Physics Research Section A. Nov2013, Vol. 728, p102-106. 5p. DOI: 10.1016/j.nima.2013.06.065.

Sand sources and transport pathways for the San Francisco Bay coastal system, based on X-ray diffraction mineralogy. Hein, James R.; Mizell, Kira; Barnard, Patrick L. Marine Geology. Nov2013, Vol. 345, p154-169. 16p. DOI: 10.1016/j.margeo.2013.04.003.

Ceremonial objects or household items? Non-destructive μ-XRD² and μ-XRF studies on three Neolithic hematite axes from Qatar. Drechsler, Philipp; Berthold, Christoph; al-Naimi, Faisal Abdallah; Eichmann, Ricardo. Arabian Archaeology & Epigraphy. Nov2013, Vol. 24 Issue 2, p119-124. 6p. DOI: 10.1111/aae.12029.

Wet sample confinement by superhydrophobic patterned surfaces for combined X-ray fluorescence and X-ray phase contrast imaging. Ciasca, G.; Businaro, L.; De Ninno, A.; Cedola, A.; Notargiacomo, A.; Campi, G.; Papi, M.; Ranieri, A.; Carta, S.; Giovine, E.; Gerardino, A. Microelectronic Engineering. Nov2013, Vol. 111, p304-309. 6p. DOI: 10.1016/j.mee.2013.02.020.

Bone quality around bioactive silica-based coated stainless steel implants: Analysis by Micro-Raman, XRF and XAS techniques. Ballarre, Josefina; Desimone, Paula M.; Chorro, Matthieu; Baca, Matías; Orellano, Juan Carlos; Ceré, Silvia M. Journal of Structural Biology. Nov2013, Vol. 184 Issue 2, p164-172. 9p. DOI: 10.1016/j.jsb.2013.09.016.

Sub-millisecond time-resolved SAXS using a continuous-flow mixer and X-ray microbeam. Graceffa, Rita; Nobrega, R. Paul; Barrea, Raul A.; Kathuria, Sagar V.; Chakravarthy, Srinivas; Bilsel, Osman; Irving, Thomas C. Journal of Synchrotron Radiation (International Union of Crystallography - IUCr). Nov2013, Vol. 20 Issue 6, p820-825. 6p. DOI: 10.1107/S0909049513021833.

Strain- and temperature-induced polymorphism of poly(dimethylsiloxane). Tosaka, Masatoshi; Noda, Miki; Ito, Kazuta; Senoo, Kazunobu; Aoyama, Koki; Ohta, Noboru. Colloid & Polymer Science. Nov2013, Vol. 291 Issue 11, p2719-2724. 6p. DOI: 10.1007/s00396-013-3044-4.

Quantification of trace arsenic in soils by field-portable X-ray fluorescence spectrometry: Considerations for sample preparation and measurement conditions. Parsons, Chris; Margui Grabulosa, Eva; Pili, Eric; Floor, Geerke H.; Roman-Ross, Gabriela; Charlet, Laurent. Journal of Hazardous Materials. Nov2013, Vol. 262, p1213-1222. 10p. DOI: 10.1016/j.jhazmat.2012.07.001.

Characterization of black volcanites from the Limay river basin, Patagonia, Argentina, using energy dispersive X-ray fluorescence spectrometry: an aid to infer human group mobility. Palacios, Oscar; Meel, Katleen; Grieken, René; Marcó P., Lué-Merú; Vázquez, Cristina. Journal of Radioanalytical & Nuclear Chemistry. Nov2013, Vol. 298 Issue 2, p1245-1255. 11p. DOI: 10.1007/s10967-013-2600-1.

Microstructural evolution of nanocrystalline chips particles produced via large strain machining during ball milling. Roshan, M.R.; Soltanpour, M.; Jahromi, S.A. Jenabali. Powder Technology. Nov2013, Vol. 249, p134-139. 6p. DOI: 10.1016/j.powtec.2013.07.028.

X-ray diffraction study on microstructures of shot/laser-peened AISI316 stainless steel. Kumagai, Masayoshi; Akita, Koichi; Itano, Yuta; Imafuku, Muneyuki; Ohya, Shin-ichi. Journal of Nuclear Materials. Nov2013, Vol. 443 Issue 1-3, p107-111. 5p. DOI: 10.1016/j.jnucmat.2013.07.010.

Polarization-Dependent Total-Reflection Fluorescence X-ray Absorption Fine Structure for 3D Structural Determination and Surface Fine Tuning. Takakusagi, Satoru; Chun, Wang-Jae; Uehara, Hiromitsu; Asakura, Kiyotaka; Iwasawa, Yasuhiro. Topics in Catalysis. Nov2013, Vol. 56 Issue 15-17, p1477-1487. 11p. DOI: 10.1007/s11244-013-0134-y.

Powder diffraction optics for SmartLab X-ray diffractometer

1. Introduction

Rigaku SmartLab is a multipurpose, fully-automated horizontal X-ray diffractometer that allows many types of measurements and evaluations of materials ranging from powders to thin films. Rigaku's expansion system and Cross Beam Optics (CBO) system enable configuration of a wide range of optics, while the SmartLab Guidance control software permits easy switching between optics for added versatility.

The many optics systems offered by Rigaku for SmartLab include CBO system incorporating a parabolic multilayer mirror, CBO-E system incorporating an elliptical multilayer mirror, and optics configured with the Kα1 unit with a Johansson Ge crystal for monochromatization of incident X-rays to the Kα1, designed to measure powder samples. These systems allow the user to configure the ideal optics for specific measurement or evaluation purposes. The new and unique Kα1 system enables various types of measurement while maintaining samples in a horizontal position.

2. CBO system

The optics of the CBO system permits easy switching of incident X-rays by simply changing the selection slit. Two systems are available: The CBO (Fig. 1) lets the user select the Bragg-Brentano focusing method or parallel beam method using a parabolic multilayer mirror, while the CBO-E (Fig. 2) lets the user select the Bragg-Brentano focusing method or convergent beam method using an elliptical multilayer mirror.

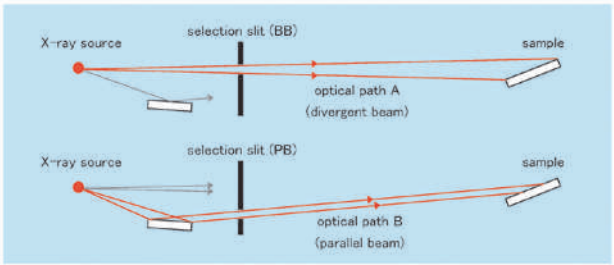

Fig. 1. Schematic diagram of CBO.

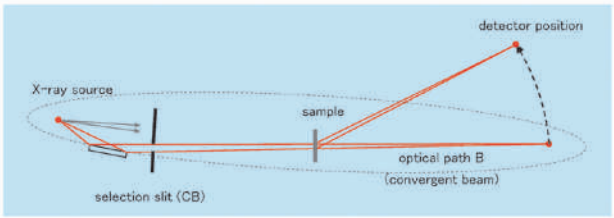

Fig. 2. Schematic diagram of CBO-E.

2.1 Bragg-Brentano optics

The Bragg-Brentano optics enables easy acquisition of high resolution and high intensity data by the reflection method (Fig. 3). It is generally used for qualitative and quantitative analysis of powder samples.

2.2 Parallel beam optics

The parallel beam optics allows accurate measurement of diffracted X-ray positions unaffected by sample shape (Fig. 4). It is generally used to analyze powder sample profiles and measure the degree of preferred orientation, as well as to measure thin-film samples.

2.3 Convergent beam optics

The convergent beam optics enables high resolution measurements by the transmission method (Fig. 5). It is used to measure samples with low absorption

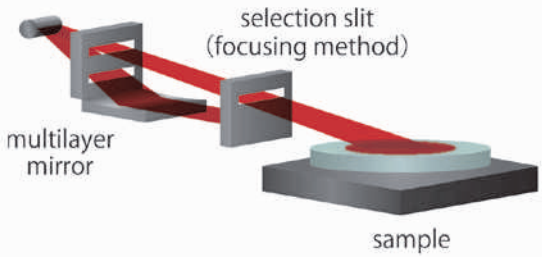

Fig. 3. Schematic diagram of CBO Bragg-Brentano optics.

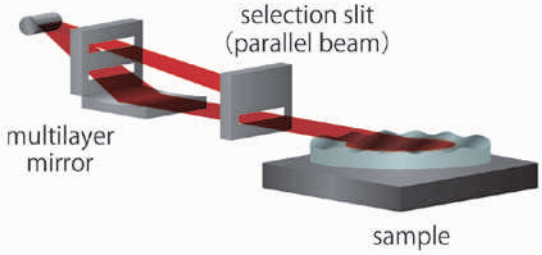

Fig. 4. Schematic diagram of CBO parallel beam optics.

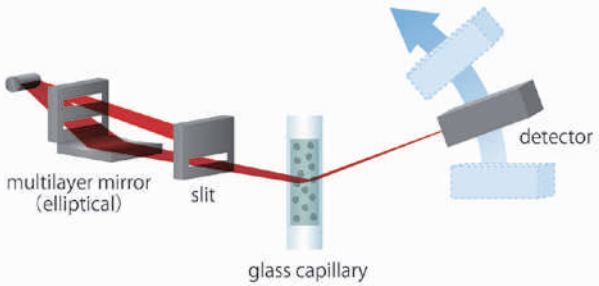

Fig. 5. Schematic diagram of CBO-E convergent beam optics.

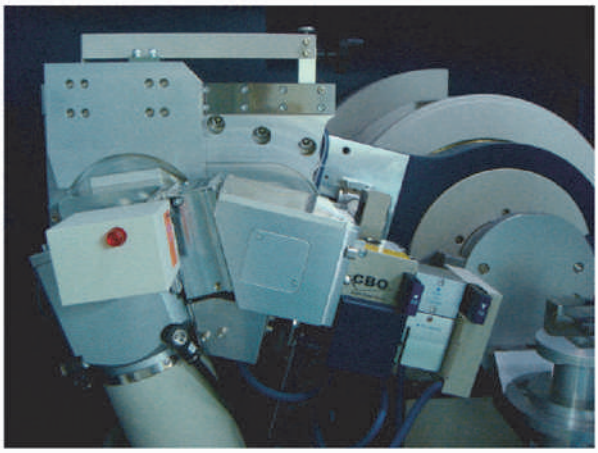

Fig. 6. Kα1 unit.

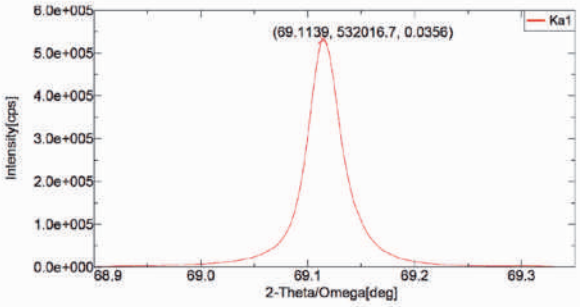

Fig. 7. Profile of Kα1 optics (Si (4 0 0)).

coefficients and preferred orientation, such as pharmaceuticals. Diffracted X-rays are focused on the detector surface for efficient measurement when combined with the D/teX Ultra 1D high-speed detector.

3. Kα1 system

Rigaku's expansion system also enables to install the Kα1 unit (Fig. 6). The user can easily switch between the conventional Kα and new Kα1 optics by installing/removing the Kα1 unit. Either of the optics can be selected depending on the purpose of measurements using your SmartLab.

Since incident X-rays are monochromatized to Kα1, even overlapped diffraction peaks can easily be decomposed. The peak positions, widths, and intensities will be determined more precisely in the diffraction patterns obtained using the Kα1 optics than using the conventional Kα1 optics. The Kα1 unit is recommended to be used for indexing or *ab initio* structure analysis, which requires high-resolution data.

4. Kα1 system+CBO system

The Kα1 system incorporates a Johansson Ge crystal for monochromatization. To allow use of the CBO system without modification, the focus position of the Kα1 system is designed to align with the conventional focus position. Simply by changing the selection slit, the user can direct X-rays monochromatized to Kα1 (Fig. 7) to Bragg-Brentano optics (Fig. 8), parallel beam optics (Fig. 9), or convergent beam optics (Fig. 10).

X-rays monochromatized to Kα1 can be used with the Bragg-Brentano focusing method and convergent beam method whereby diffracted X-rays are focused on the detector surface for efficient measurement when combined with the D/teX Ultra 1D high-speed detector. Compared to conventional monochromatization methods, this achieves faster high intensity measurements. Pairing the Kα1 unit with the CBO system lets users configure the ideal optics for the specific purpose of a measurement or analysis.

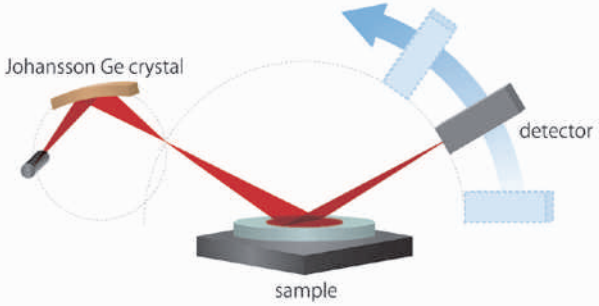

Fig. 8. Schematic diagram of Kα1 unit+Bragg-Brentano focusing method.

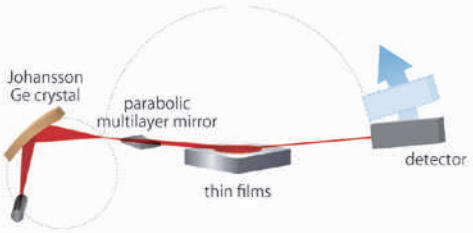

Fig. 9. Schematic diagram of Kα1 unit+parallel beam method.

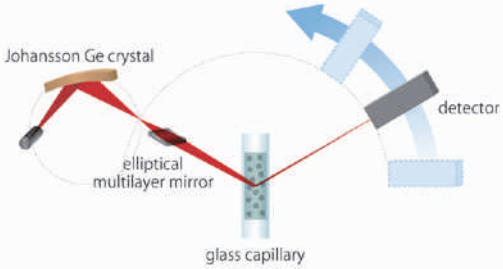

Fig. 10. Schematic diagram of Kα1 unit+convergent beam method.

Return to eNewsletter

Rigaku

Application Note XRF 5018

Silicate Rock Analysis by the Low Dilution Fusion Method

Application

silicate rock,
petrology,
geology

Instrument

Wavelength dispersive
X-ray fluorescence
spectrometer
ZSX PrimusII

Keywords

silicate rock,
trace element
fusion method

Introduction

The measurement of geochemical data from silicate rocks is essential for modern petrology. Concentrations of major and trace components in igneous rock samples provide many kinds of information about rock history such as eruption or solidification, magma evolution, magma genesis and source materials as well as petrographical classification.

X-ray fluorescence spectrometry for silicate rock analysis has been developed over the last few decades. The XRF technique is currently used as a standard analytical method to determine the chemical composition of major elements in silicate rocks.

Highly accurate rock analysis requires use of the fusion method to eliminate sample heterogeneity, such as grain size and mineralogical effects, owing to various rock-forming minerals. The conventional fusion method has been predominantly used for the determination of major elements in silicate rock because the dilution by flux significantly reduces sensitivities for measuring trace elements. The pressed powder method is, therefore, applied to trace element analysis. Since it is time-consuming and not very efficient to use two preparation methods for one sample, a low dilution fusion method was developed. The low dilution fusion bead technique is a method for improving trace element sensitivity, enabling the determination of concentrations of trace elements as accurately and reliably as well as the major element determination by XRF.

This note demonstrates this advanced method for determining the chemical composition of silicate rocks by XRF.

Instrument

The ZSX PrimusII is floor-standing sequential wavelength dispersive X-ray fluorescence (WDXRF) spectrometer. WDXRF has the advantage of high spectral resolution and high sensitivity for light elements. The ZSX PrimusII is designed to provide reliable analysis results and its flexibility provides multipurpose usability for a wide range of applications.

The ZSX PrimusII is equipped with a high performance 4 kW Rh target X-ray tube with an ultra-thin beryllium window. This tube provides unconventional high sensitivity for light element analysis. Analyzing crystals allow measurement from beryllium to uranium.

The instrument also has a built-in intelligent auto sample changer (ASC). The ASC is upgradable up to a 48-sample stage if needed.

The ZSX PrimusII has a unique optical configuration designed to minimize errors caused by an uneven bead surface. It enables measurement of fused beads with high precision where the surface becomes curved by deformation of a platinum crucible, which has been in continuous fusion operation.

Operation software provides non-specialist users with easy-to-use operation. In particular, a software flowbar design fully supports the user's operation of setting-up quantitative analysis, making a tedious task, easy to do.

Sample and sample preparation

The standard samples used for calibration were 14 certified reference materials (CRMs) supplied from the Geological Survey of Japan (GSJ). These standards are composed of basic to acidic igneous rocks. Range of SiO2 content in these CRMs ranges from 43.6 to 76.8 in mass%.

The well-dried (2 hours at 105 degrees C) samples were fused with a mixed flux of Spectroflux 100B (4LiBO2:1LiB4O7) supplied from Johnson Matthey with sample to flux ratio 1:2 by using a fusion machine.

Measurement

The ZSX PrimusII with 4kW Rh target X-ray tube was used for measurement. Each measurement was performed with the tube at maximum power. All of the trace elements were measured with a primary beam filter to reduce background. Counting times for the rare earth elements were 400 – 800 seconds and for the other trace elements, 100 – 200 seconds.

Matrix correction coefficients (alpha) in the calibration were theoretically calculated by built-in FP software. In the calculation of theoretical alpha, ignition loss was set as a balanced component.

Results

Calibration curves for the major elements are shown in Figure 1. Accuracy of SiO2 is less than 0.2 in such a wide concentration range. Other calibration curves

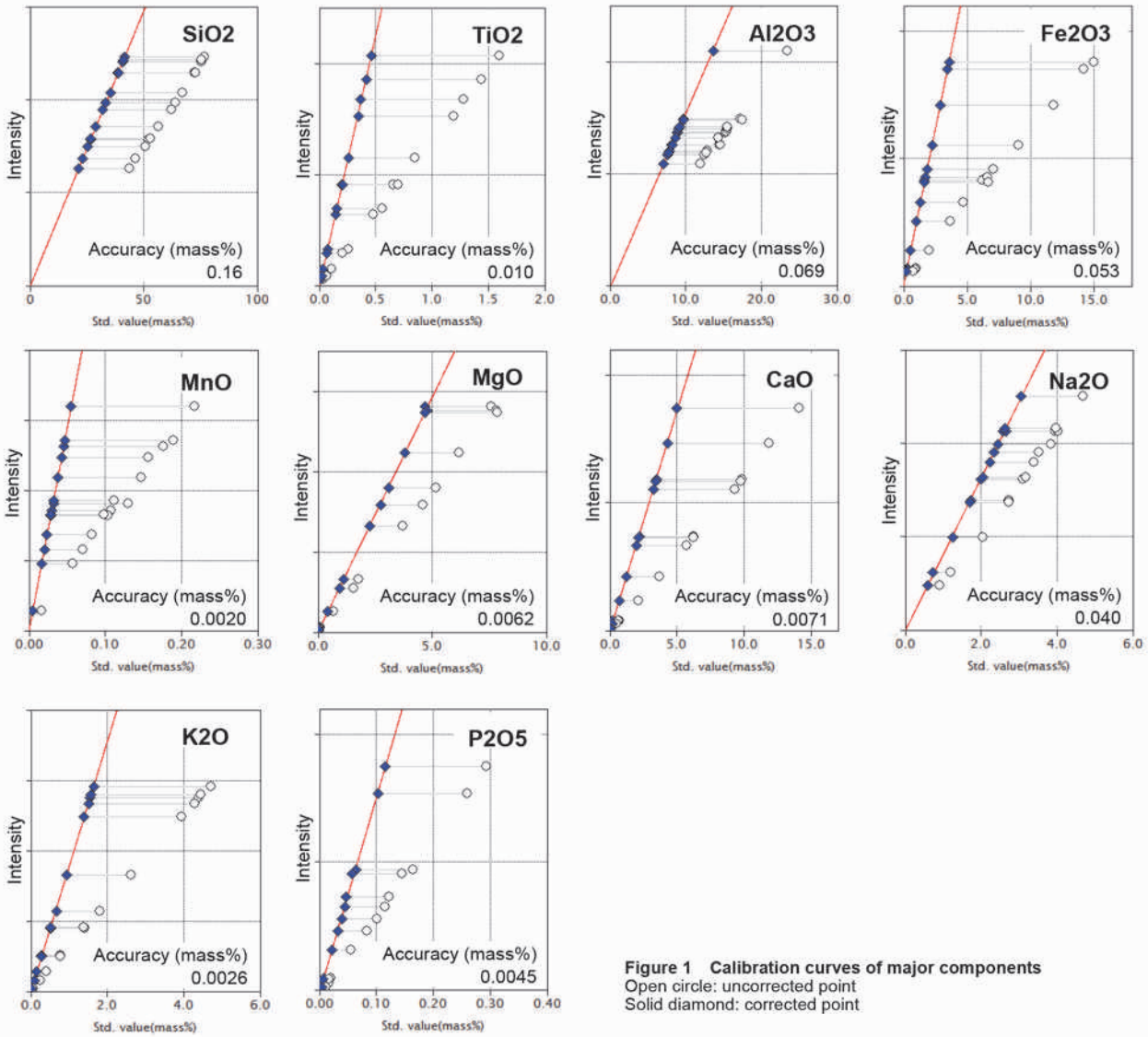

Figure 1 Calibration curves of major components
Open circle: uncorrected point
Solid diamond: corrected point

also show excellent accuracy.
The accuracy is calculated using the following formula.

$$\text{Accuracy} = \sqrt{\frac{\sum_i \left(C_i - \hat{C}_i\right)^2}{n - m}}$$

C_i : calculated value of standard sample i
$\hat{C}_i$: reference value of standard sample i
n : number of standard samples.
m : degree of freedom (linear 2, quad. 3)

Typical lower limits of detection (LLD) and typical accuracy of calibration curves for each trace element are shown in Table 1. The LLDs are calculated as follows:

$$\text{LLD} = 3 \cdot 1/m \cdot \sigma_B = 3 \cdot 1/m \cdot \sqrt{\frac{I_B}{1000 \cdot t}}$$

m : sensitivity of calibration (kcps/mass%)
σ_B : standard deviation of blank intensity (kcps)
I_B : intensity of the blank (kcps)
t : counting time (s); 100 s is used

Table 1 Typical LLD and accuracy of calibration curve for trace elements

unit : ppm

Component / Element	Typical LLD (100s, 3σ)	Typical accuracy
Ba	4.5	12.9
Ce	1.9	2.5
Co	0.2	1.3
Cr	0.5	2.5
Cu	0.2	5.9
Ga	0.2	0.6
La	1.9	2.4
Nb	0.5	1.1
Nd	4.2	2.5
Ni	0.2	3.3
Pb	0.1	0.5
Rb	0.1	3.5
Sc	0.5	3.7
Sm	2.5	1.3
Sr	0.1	4.6
Th	0.2	1.3
V	0.8	3.9
Y	0.1	0.6
Yb	1.3	0.7
Zn	0.1	1.7
Zr	0.1	6.0

The ultra thin window, 4 kW high-power X-ray tube of ZSX PrimusII is a great advantage in the determination of trace elements.
To test instrumental precision, 20 repetitive measurements were performed with a granodiorite sample (JG-3). The results of the average and standard deviations of each component are shown in Table 2.

Table 2 Result of precision test

unit : ppm

Component / Element	Certified value	Average of 20 meassurement	Std. dev.	RSD%
SiO2 (mass%)	67.29	67.05	0.037	0.054
TiO2 (mass%)	0.48	0.48	0.002	0.34
Al2O3 (mass%)	15.48	15.50	0.012	0.074
T.Fe2O3 (mass%)	3.69	3.71	0.004	0.096
MnO (mass%)	0.071	0.071	0.0004	0.62
MgO (mass%)	1.79	1.80	0.007	0.40
CaO (mass%)	3.69	3.67	0.004	0.10
Na2O (mass%)	3.96	4.02	0.018	0.44
K2O (mass%)	2.64	2.61	0.002	0.086
P2O5 (mass%)	0.122	0.128	0.0008	0.63
Ba	466	469	6.2	1.3
Ce	40.3	38	1.7	4.5
Co	11.7	11	0.38	3.4
Cr	22.4	23	0.80	3.5
Cu	6.81	6	0.34	6.1
Ga	17.1	16	0.37	2.3
La	20.6	21	1.5	7.2
Nb	5.88	8	0.23	2.9
Nd	17.2	16	0.82	5.3
Ni	14.3	15	0.32	2.1
Pb	11.7	11	0.45	4.0
Rb	67.3	71	0.28	0.40
Sc	8.76	9	0.99	10
Sm	3.39	3	0.56	19
Sr	379	367	0.45	0.12
Th	8.28	9	0.30	3.5
V	70.1	68	1.4	2.0
Y	17.3	18	0.20	1.1
Yb	1.77	2	0.28	18
Zn	46.5	46	0.34	0.74
Zr	144	152	0.29	0.19

Conclusions

X-ray fluorescence spectrometry is a rapid, precise and accurate method to meet the requirements of silicate rock analysis. It can also minimize the necessary skill and time for sample preparation compared to other spectroscopic analysis methods, which use a wet chemical technique.

This note describes an XRF method utilizing the low dilution fusion technique applied to silicate rock samples which allows the determination of major elements to trace elements with high accuracy.

This method covers almost all trace elements required for modern geochemical investigations. It also covers some rare earth elements.

XRF analysis is the best method to obtain accurate and precise fundamental data required for scientific study in petrology and geochemistry. The method is also widely applicable for geological matters, such as environmental assessment of soil, exploring resources and process and quality control in mining as well as scientific investigations.

Return to eNewsletter

Rigaku

Rigaku Corporation Tokyo Branch
4-14-4, Sendagaya, Shibuya-ku, Tokyo 151-0051, Japan
Phone +81-3-3479-0618 Fax +81-3-3479-6112 rinttyo@rigaku.co.jp

www.Rigaku.com

Rigaku Corporation
Head Office
3-9-12, Matsubara-cho, Akishima-shi, Tokyo 196-8666, Japan
Phone +81-42-545-8189 Fax +81-42-544-9223
rinttyo@rigaku.co.jp

Rigaku Corporation
Osaka Factory
14-8, Akaoji-cho, Takatsuki-shi, Osaka 569-1146, Japan
Phone +81-72-693-7990 Fax +81-72-693-6746
rinttyo@rigaku.co.jp

Rigaku Americas Corporation
9009 New Trails Drive, The Woodlands, Texas 77381-5209, USA
Phone +1-281-362-2300 Fax +1-281-364-3628
info@rigaku.com

Rigaku Beijing Corporation
2601A, Tengda Plaza, No.168, Xizhimenwai Avenue,
Haidian District, Beijing 100044, P.R.China
Phone +86-010-8857-5768 Fax +86-010-8857-5748
info@rigaku.com.cn

Rigaku Europe SE
Gross-Berliner Damm 151, 12487 Berlin, Germany
Phone +49-30-6264035-0 Fax +49-30-6264035-10
rese@rigaku.co.jp

Rigaku

THE BRIDGE

MATERIALS ANALYSIS eNEWSLETTER

NOVEMBER 2013, ISSUE 5

Rigaku Corporation and its Global Subsidiaries
website: www.Rigaku.com | email: info@Rigaku.com